Asociación Argentina
de Mecánica Computacional

Mecánica Computacional Vol XXXIII, págs. 1751-1765 (artículo completo)
Graciela Bertolino, Mariano Cantero, Mario Storti y Federico Teruel (Eds.)
San Carlos de Bariloche, 23-26 Setiembre 2014

DYNAMIC ANALYSIS OF A GUYED MAST WITH UNCERTAINTIES ON THE GUY INITIAL TENSION AND THE WIND LOAD

Jorge S. Ballaben[a,b], Marta B. Rosales[a,b] and Rubens Sampaio[c]

[a]*Departamento de Ingeniería, Universidad Nacional del Sur, Bahía Blanca*

[b]*CONICET*

[c]*Departamento de Ingeniería Mecánica, Pontificia Universidade do Rio de Janeiro, Brazil.*

Keywords: Guyed structures, stochastic wind load, uncertainties quantification, dynamic analysis, reduced order model.

Abstract. The dynamic response of a guyed mast is analyzed under wind load action. The structural model consists of a beam-column model accounting for the second order effect due to axial loads and one guy. The guy is represented by an extensible cable governed by nonlinear equations. The wind velocity is derived considering temporal and spatial correlations. The resulting governing system is discretized using finite elements and a reduced order model is afterwards developed using normal modes as a basis. The wind load is obtained from a stochastic wind velocity field and derived using the Spectral Representation Method. Usually, the design tension changes during the structure service life affecting the system performance. As the guy pretension is a significant parameter in the behavior of guyed structures, its variation is a relevant issue. Then, an uncertainty quantification appears necessary to obtain more realistic results. Since the nonlinear structures shows special sensitivity to the load, the mean value of wind velocity (used to construct the wind loads), is also considered as a stochastic parameter.

1 INTRODUCTION

For many years, guyed masts have been used to support antennas for radio, TV and other types of communication (Fig. 1(a)). This structure has clear advantages in the open country, where there are no restrictions on the position of the cable anchors. However, it can also be found in urban areas, due to its low cost compared with other typologies. A typical configuration comprises a lattice tower with triangular cross-section (three legs, horizontal and diagonal members). The height is variable depending on the functions, but nowadays is not exceptional to see 300 m-height towers. The main structural characteristics are the large slenderness of the mast and several levels of taut guys. Dynamic actions as wind, are usually simplified as quasi-static loads that represent the mean of the dynamic phenomena amplified with factors that account for the dynamics characteristics at each case, following standard codes and recommendations. Since wind load contains energy that interacts with flexible structures, the dynamic response becomes important in the analysis of guyed masts. The mast acts strongly in a nonlinear fashion when the guys vary between slack and taut states.

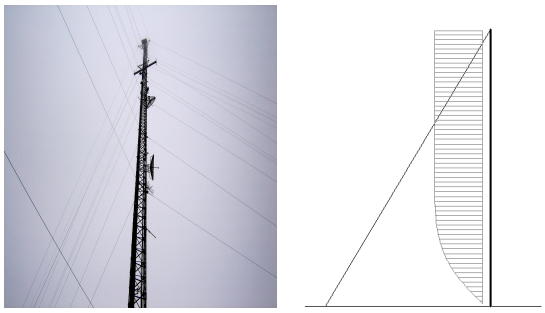

(a) (b)

Figure 1: (a) Typical guyed tower for mobile signal transmission. (b) Reduced model studied.

Despite the large potential of adverse impact, dynamic actions, as wind and earthquakes, are not addressed in detail with exception of special cases (e.g.Preidikman et al. (2006)). Works of other authors show that the guyed structures have special sensitivity to the type and amplitude of the excitation (Lenci and Ruzziconi (2009)), even avoiding the resonace effects. In this work, the dynamic response of a reduced and simplified model of a guyed tower is analyzed under wind loads. The fluctuating wind component is obtained through the Spectral Representation Method (SRM) (Shinozuka and Jan (1972)) starting from a given Power Spectral Density function (*psdf*). The temporal and spatial correlations are taken into account by finding the cross-spectrum and introducing a coherence function. The method yields a temporal record of the fluctuating wind velocity. Combined with the standard recommendations, the fluctuating wind pressure are applied on the mast. Using the classical extended Hamilton's principle, the equations of motion that govern the transverse vibration are obtained. Then, a finite element discretization of the linerized equations is used to perform a modal analysis of the structure. Finally, by means of a Galerkin Method, the main nonlinear PDE system is reduced into a 2-DOF model, using two selected normal modes extracted from the previous modal analysis. With this reduced order model (ROM), the nonlinear response of the structure, excited by a stochastic wind load is evaluated, considering uncertainties on the initial pretension of the guy and the mean wind velocity.

2 MODEL DESCRIPTION

2.1 Problem formulation

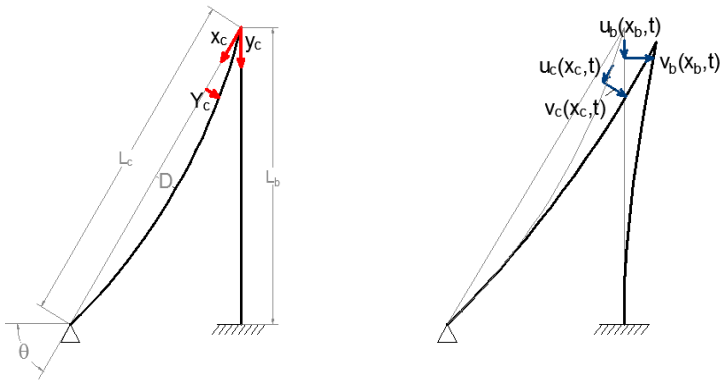

(a) (b)

Figure 2: Cable-stayed tower configurations: a) static; b) dynamic.

The plane configuration of a guyed column (see Fig 2) is described, referenced to the static equilibrium state, by the cable displacement components $u_c(x_c,t)$ and $v_c(x_c,t)$ along the abscissa x_c, and by the beam-column transverse displacements $v_b(x_b,t)$ and $u_b(x_b,t)$ along x_b. The following assumptions are made: a) both the cable and the beam-column are considered as homogeneous one-dimensional elastic continua obeying a linear stress-strain relationship; b) the equilibrium configuration for the inclined cable is described through a quadratic parabola under the assumptions of small sag to length ratio; c) axial extensions of the cable are described by the Lagrangian strain of the centerline; d) the flexural, torsional and shear stiffness of the cable are negligible; e) the torsional and shear strain of the beam are negligible; f) the nonlinearity of the problem arises from the cable formulation; g) a second order effect due of the axial load (assumed constant) is accounted for in the column equation. The cable formulation follows the approach reported by Gattulli and Lepidi (2007). Under these assumptions and by using the classical extended Hamilton's principle, the equations of motion governing the transverse vibration of the guyed column are obtained:

$$\begin{cases} V_b : m_b\ddot{v}_b + c_b\dot{v}_b + EIv_b'''' + P_H v_b'' = F_{v_b}(t,x_b) \\ U_b : m_b\ddot{u}_b + c_b\dot{u}_b + EA_b u_b'' = F_{u_b}(t,x_b) \\ V_c : m_c\ddot{v}_c + c_c\dot{v}_c - [Hv_c' + EA_c(Y_c' + v_c')\epsilon_c]' = F_{v_c}(t,x_c) \\ U_c : m_c\ddot{u}_c + [EA_c\epsilon_c]' = F_{u_c}(t,x_c) \end{cases} \tag{1}$$

with the following set of geometric and mechanical boundary conditions:

$$\begin{cases} u_c(l_c) = v_c(l_c) = 0 \\ v_b(l_b) = v_b'(l_b) = u_b(l_b) = 0 \\ EIv_b''(0) = 0 \\ v_b(0) = -u_c(0)\cos\theta + v_c(0)\sin\theta \\ u_b(0) = u_c(0)\sin\theta + v_c(0)\cos\theta \\ EIv_b'''(0) + (EA_c\epsilon_c + H)\cos\theta + [EA_c\epsilon_c(y_c'(0) + v_c'(0)) + Hv_c'(0)]\sin\theta = 0 \end{cases} \tag{2}$$

Here $(*)' = d(*)/dx_c$ and $\dot{(*)} = d(*)/dt$, m_b and m_c denote the beam and cable mass per unit length, respectively, $EI = E_bI_b$ the beam flexural stiffness, P_H is the component of the initial pretension in the direction of the mast, $EA_c = E_cA_c$ and $EA_b = E_bA_b$ the cable and beam axial stiffness, respectively, H is the mean static tension in the cable, Y_c is the initial configuration of the cable and, due the hypothesis of small sag to span ratio, $Y_c(x_c) = 4D(X_c/l_c - (X_c/l_c)^2)$, finally $\epsilon_c = u_c + y_c'v_c' + 1/2v_c'^2$ is the expression of the elongation for the cable. Since in cable-stayed structures the beam and the cable materials can generally have different viscous behavior, the model accounts separately for beam and cable transverse damping per unit length, C_b and C_c respectively; here an estimate of system damping is assumed to give the conventional values $c_i = 8.5e^{-3}(2m_i\omega_i)$, with $i = c, b$ and ω_i is a natural frequency of the system. Here w_i is chosen by observation of the modal shapes used in the approximation, i.e. if the modal shape selected is a cable-like mode, then the corresponding frequency is used to the damping term of the cable; the value of w_i were found with H = 10500 N.

The values of the constants for the problem are detailed in Tab. 1.

Table 1: Values of the constants for Eqs. (1-2)

l_b	E_b	I_b	A_b	m_b	l_c	E_c	A_c	m_c	H
30	$2.1e^{11}$	$8.33e^{-4}$	0.04	314	32.31	$1.5e^{11}$	$7.854e^{-5}$	0.61	$7000 - 14000$
m	N/m^2	m^4	m^2	kg	m	N/m^2	m^2	kg	N

2.2 Weak formulation and Finite Element discretization.

After stating the weak formulation for the guyed column, the governing system of equations 1 is discretized by means of a ad-hoc finite element formulation. The column is modeled using 6-DOF beam elements and the cable using 6-DOF (three node) cable elements. Figure 3 depicts three selected modal shapes found with a modal analysis.

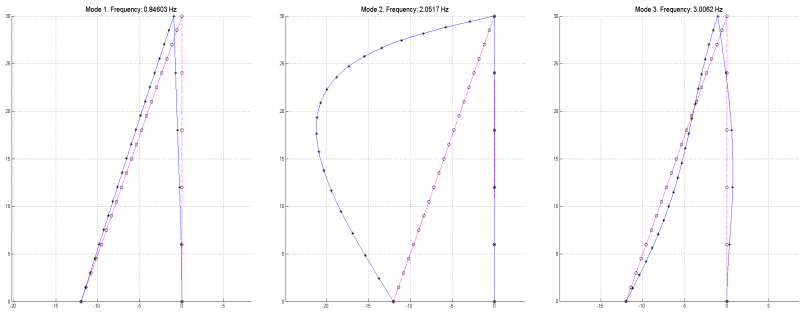

(a) (b) (c)

Figure 3: Results of FEM modal analysis

2.3 Galerkin projection and reduced order model (ROM)

By means of a Galerkin Method, the main nonlinear equations system is further reduced into a 2-DOF model, using two selected normal modes extracted from the previous modal analysis. With this ROM the nonlinear response of the structure, excited by a stochastic wind load is evaluated, considering the uncertainty of the initial pretension on the guy. The 2-DOF ROM has been previously verified with an analogous finite element model from a commercial software and reproduces correctly the amplitude, shape and frequency as seen in Fig 4. The small shift of

around the 1% in the main frequency is thought to be related to the differences in the damping model used in both the commercial model and the ROM here presented.

The displacements have been expressed in the modal space as $v = \mathbf{\Phi} q$ where the displacement vector is ordered as $v = \{v_b(x_b,t), u_b(x_b,t), v_c(x_c,t), u_c(x_c,t)\}^T$, the modal matrix $\mathbf{\Phi} = [\boldsymbol{\phi}_1 | \, \boldsymbol{\phi}_2]$ is composed by the eigenfunctions $\boldsymbol{\phi}_i = \{\phi_{b_v i}(x_b), \phi_{b_u i}(x_b), \phi_{v_c i}(x_c), \phi_{u_c i}(x_c)\}^T$ and the modal amplitude vector is $\boldsymbol{q} = \{q_1(t), q_2(t)\}^T$ Imposing the stationarity of the associated Hamiltonian, the following nonlinear ordinary differential equations in terms of the generalized coordinates q_1 and q_2 are obtained:

$$\begin{cases} m_1\ddot{q}_1 + a_1\dot{q}_1 + c_1 q_1 + c_2 q_2 + c_{12} q_1 q_2 + c_{11} q_1^2 + c_{22} q_2^2 + c_{211} q_1^2 q_2 + c_{122} q_1 q_2^2 + \\ \qquad + c_{111} q_1^3 + c_{222} q_2^3 = p_1(t) \\ m_2\ddot{q}_2 + a_2\dot{q}_2 + d_1 q_1 + d_2 q_2 + d_{12} q_1 q_2 + d_{11} q_1^2 + d_{22} q_2^2 + d_{211} q_1^2 q_2 + d_{122} q_1 q_2^2 + \\ \qquad + d_{111} q_1^3 + d_{222} q_2^3 = p_2(t) \end{cases} \tag{3}$$

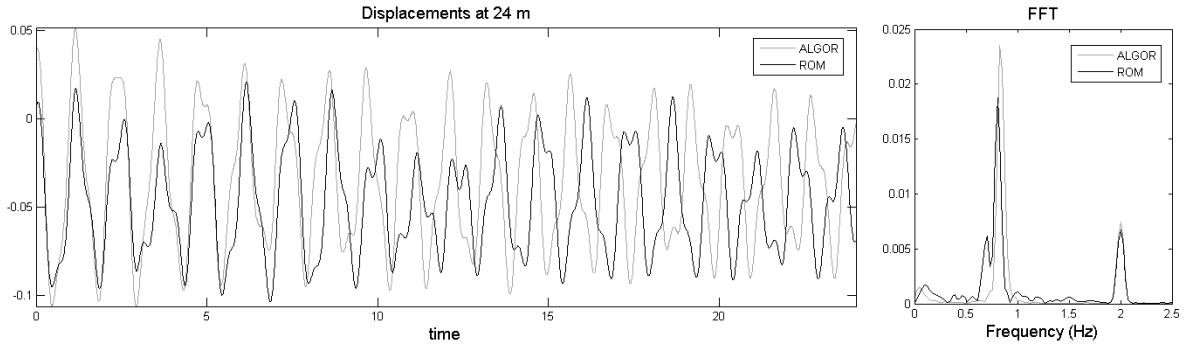

Figure 4: Verification of the ROM model

2.4 Wind load

In this work, a wind load with a mean varying with the height (y coordinate, see Fig. 2) in a potential law fashion (see Fig 1(b)) given by the standards, and with a temporal variation generated by means of the Spectral Representation Method (SRM) Shinozuka and Jan (1972) is applied on the structure. The wind load takes into account both temporal and spatial correlations. Following the SRM, a signal that verifies the assumptions of a homogeneous, ergodic and Gaussian process with zero mean, and under certain conditions, can be recreated by the following series:

$$u_y(t) = \sum_{k=1}^{m} \sum_{n=1}^{N} |H_{yk}(w_n)| \sqrt{2\Delta w} \cos[\hat{w}_n t + \theta_{yk}(w_n) + \Phi_{kn}] \tag{4}$$

where Δw is the frequency interval with which the *psdf* is discretized, $w_n = \Delta w(n-1)$, $\hat{w}_n = w_n + \psi_{kn}\Delta w$, ψ_{kn} is a random value uniformly distributed between 0 and 1, N is the amount of frequency ranges and, Φ_{kn} are the random independent phase angles uniformly distributed between 0 and 2π. If the values of S_{jk} are all real, then the $\theta_{jk}(w_n)$ are equal to zero. The lower triangular matrix $H(w)$ is obtained by means of the *Cholesky Decomposition* of the spectral density matrix.

3 UNCERTAINTIES QUANTIFICATION

The uncertainty quantification isperformed with one parameter: the initial pretension of the guys (cable tension). Then, the stochastic feature of the problem is given by the initial pretension. Monte Carlo simulations are carried out by taking the initial cable pretension (H) as a random variable. A Gamma probability density function is derived using the Principle of Maximum Entropy (PME) (Shannon, 1948). The PME states that, subject to known constraints, the PDF which best represents the current state of knowledge is the one with largest entropy. The measure of uncertainty of a random variable X is defined by the following expression

$$S(f_X) = -\int_D f_X(X) log(f_X(X)) dX \tag{5}$$

in which f_X stands for the PDF of X and D is its domain. It is possible to demonstrate that the application of the PME under the constraints of positiveness and bounded second moment, leads to a Gamma PDF. The cable tension fulfill these conditions.

The Gamma distribution Eq. 6 with parameters a and b, where $E(X) = ab$; $\sigma_X = ab^2$, is given by the next expression

$$f(x) = \frac{1}{b^a \Gamma(a)} x^{a-1} e^{\frac{-x}{b}}. \tag{6}$$

Consequently, H is distributed according to a Gamma distribution, where the mean and standard deviation (SD), will be specified. Afterwards, Monte Carlo simulations are performed in order to find the influence of this variation on the response of the structure. To achieve significant statistical results, a convergence study on the standard deviation was performed to determine the minimum number of realizations of the Monte Carlo simulations. It was found that at least 2000 realizations are required to achieve convergence of the standard deviation. The range of values of initial pretension was chosen following the standard codes suggestions.

4 ANALYSIS OF THE RESULTS

4.1 Deterministic analysis of the response

In this work, for sake of brevity, only results on transversal displacements on the beam are presented. The total time of calculations was 180 s. Figure 5 depicts a sample of the transverse displacement temporal variation for the extreme cases of initial pretensions and for $V_m = 55$ m/s. It can be seen that the overall response has smaller amplitudes for higher values of H, as expected, but also shows a very different shape. A particular frequency of vibration can be recognized at each of the depicted records, while the amplitude of the oscillation exhibits a non-periodic behavior. These observations hold for all the time history results for the displacements.

A FFT study was performed to know the content of frequency of the time history responses. The Figure 6 (b) shows two typical FFT, for the extreme cases of V_m and for the maximum value of H. It can be seen that for the smallest mean wind velocities, the frequency content is narrow and concentrated in one frequency (although the response is not periodic) and when the value of V_m increases, several peak frequencies appear, and their values are lower. The other cases (not showed here) are intermediate between the two depicted; the range of the most important frequency content of all the cases belongs to the $0.5 - 0.85$ Hz zone. Figure 6 (a) illustrates the variation of the maximum peak frequency of the FFT for all the H and V_m combinations. It can be seen that the greater variations are due the V_m parameter, although H has some relative importance.

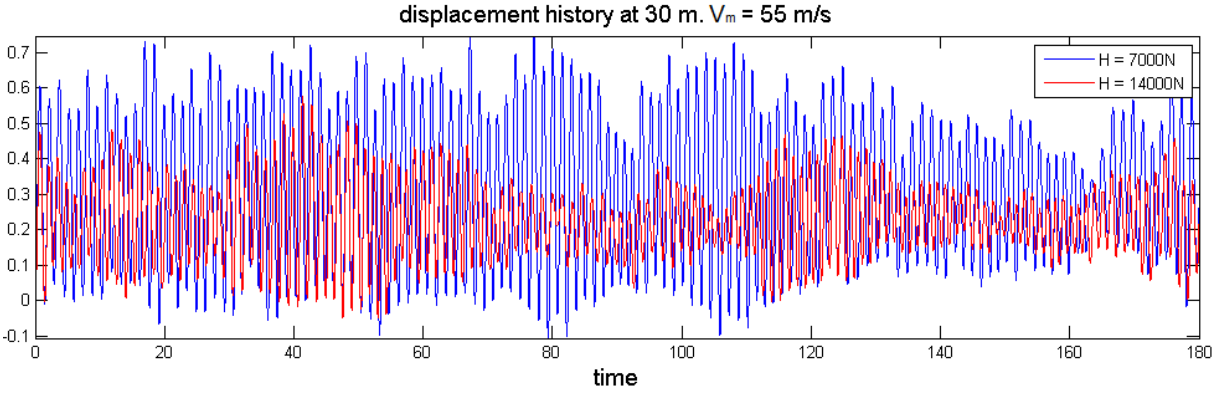

Figure 5: Time history of the transverse displacement of the beam-column at point $x_b = 0m$ (tip of the mast) found with the deterministic reduced order model for the extreme cases of H.

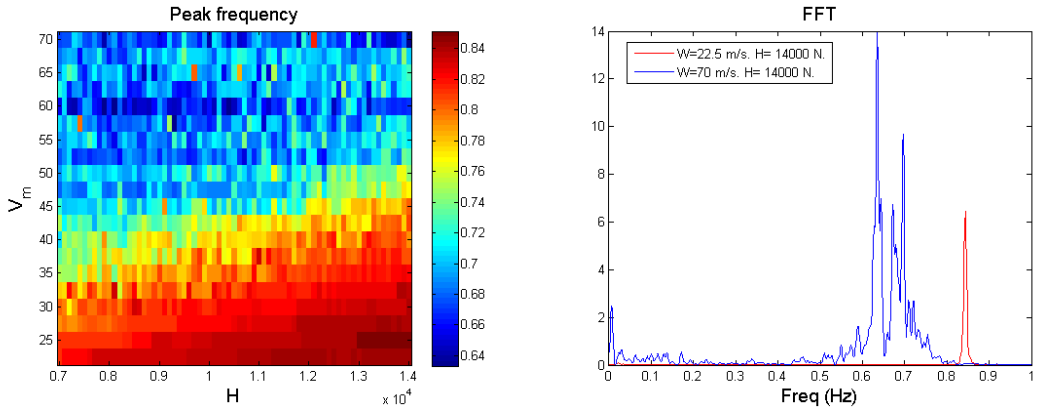

(a) (b)

Figure 6: Frequency analysis of the transverse displacement of the beam-column at point $x_b = 0m$ (tip of the mast) found with the deterministic reduced order model for all the combinations of H and V_m. (a)Mosaic plot of the peak frequency. (b) Examples of FFT.

In Fig. 7 (a) a typical phase plane is depicted, Fig. 7 (b) shows the Poincaré map, when the phase plane is sampled at the period corresponding to the peak frequency of the FFT analysis. From both figures it is clear that a periodic attractor is not present, though it is not possible to ensure that the motion is chaotic or if any other nonlinear bifurcation is present, without a deeper analysis.

Figure 8 illustrates the variation of the maximum and mean values of the displacements at the tip of the mast for each case of H and V_m. The parameter V_m shows a larger influence over these measures. Both Figs (a) and (b), show a similar variation, despite that in the Fig. (a) the results have more dependency on H but in a less predictable way.

Figure 9 depicts the percentage of time (of the total calculated) that the displacements exceed a value of 0.40 m, that could be an operational limit. It is clear that, for the lower values of V_m , the response never exceeds the limit. Abruptly and around the band of $V_m = 50$ m/s an exceedance of 5-15 % can be observerd and rapidly increasing with small increases of V_m. The value of H has some influence in general terms.

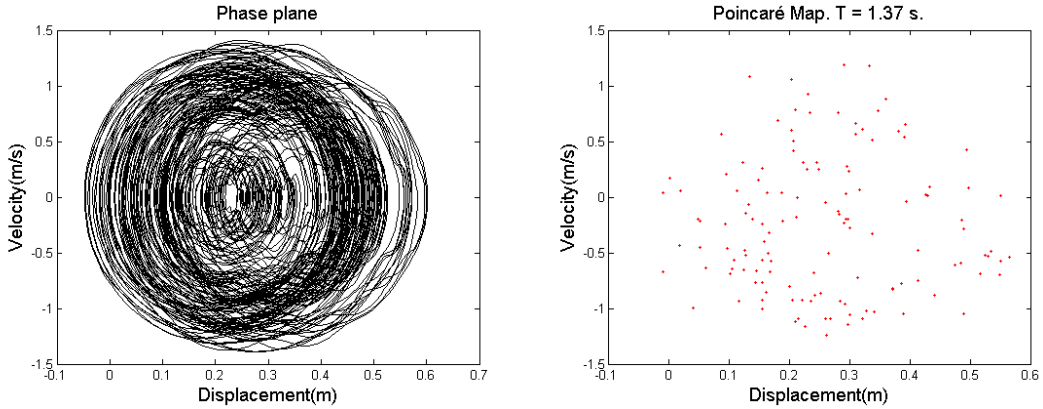

(a) (b)

Figure 7: A typical phase plane (a) and Poincaré map (b) of the transverse displacement of the beam-column at point $x_b = 0m$ (tip of the mast) found with the deterministic reduced order model.(This case corresponds to $H = 10400N$ and $V_m = 55m/s$)

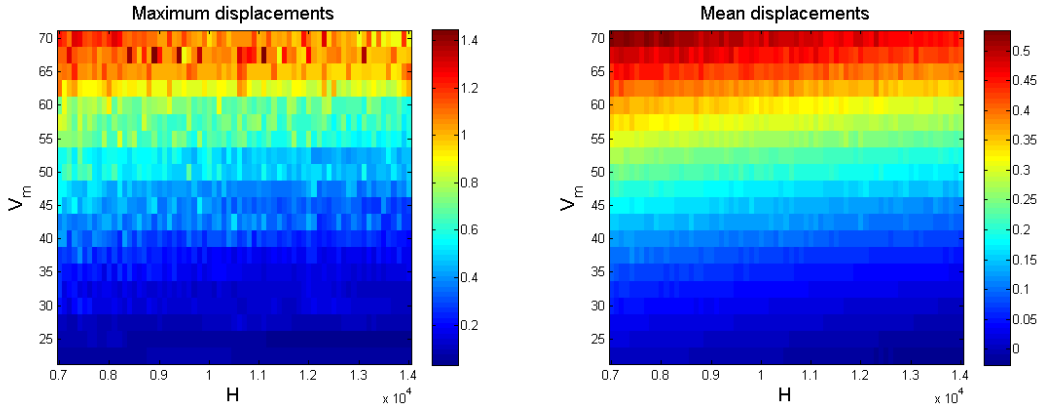

(a) (b)

Figure 8: Maximum (a) and mean (b) of the transverse displacement of the beam-column at point $x_b = 0m$ (tip of the mast) found with the deterministic reduced order model for all the combinations of H and V_m.

4.2 Statistical analysis of the response

Figure 10 illustrates the contour plots of correlations between time realizations for all the values of H and four cases of V_m. The white color indicates full correlation and the black color indicates the zero correlation (no anti-correlation is observed). In the Fig. 10 (a) (that corresponds to the lowest V_m studied), some good correlation between results in a thin zone around the diagonal can be seen, and it exhibits two zones of wider good correlation for approximately the 30% lowest and highest values of H. Fig. 10 (b) has three zones of good correlation, despite the two corresponding to the lowest values of H are very small. Figs 10 (c) and (d) depict poor or none correlations between results, even around the diagonal. When the correlation for a fixed value of H and for all the cases of V_m, plots like Fig. 10 (d) are obtained. From this analysis, it can be concluded that, for mean to high values of V_m, the shape of the time history of displacements has high sensitivity on V_m and H and the evolution of the results do not follow any linear relationship, even when results for close values of H and V_m are compared.

Next, the results analyzed statistically will be discussed. A Gamma probability density func-

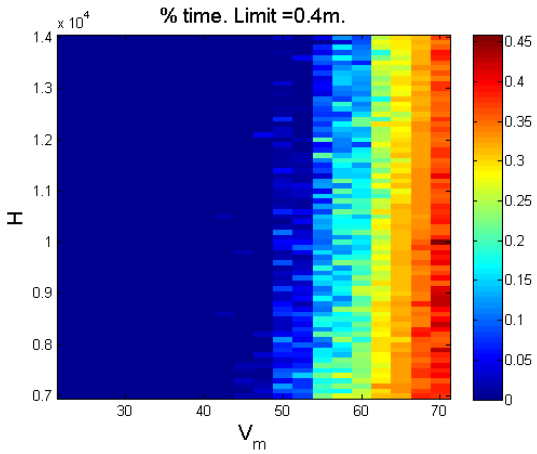

Figure 9: Percentage of time that the transverse displacement of the beam-column exceeds the limit value of 0.40m at point $x_b = 0m$ for all the combinations of H and V_m.

tion (PDF) is used for the Montecarlo simulations (see Section 3). A convergence study was carried out to determine the optimum number of simulations that are necessary to achieve statistical accuracy and it was found that at least 2000 realizations were necessary. Once the realizations were finished, the PDF graphs were constructed using the *ksdensity* function of MATLAB, that estimate the PDF of a set of data using the *kernel* method. The bandwidth for the kernel function (here a normal function is used), is optimized in MATLAB, and it is useful when the target PDF is normal, but may give wrong results when that condition is not fulfilled. In this work, after several tests, and following an engineering criterion, the authors adopted a bandwidth of 5cm, that gives as result smooth PDFs and allows to observe multimodalities, when the modes are separated enough to be of engineering interest.

Each time history of displacements (here only the displacements at the tip of the mast are studied) can be tackled as a stochastic process, since the wind load is a stochastic process itself, even assuming H and V_m deterministic. In Fig. 11 (a), a 3D surface that depicts the evolution of the PDF of the displacements with H is showed, for a fixed value of $V_m = 70$ m/s. In Fig. 11 (b) a top view of that surface is illustrated, along with the 5% and 95% (cubic interpolated) confiability bands. Fig. 11 (c) plots some specific PDFs as examples of the various types that appears. It can be seen from Fig 11 (b) that the mean is almost constant with H (the same result observed in Fig 8 (b)) and the width of the bands get narrow for higher values of H. Some cases of multimodality are also found, as depicted in blue in Fig. 11(c). The shape of the PDF of the displacements records results very variable with H, ranging from pointed and centered to a flat or multimodal cases.

Figure 11 shows from a similar point of view that the Fig. 11. The PDF of displacements records for each value of V_m and for a fixed value of $H = 7000$ N. It can be seen from Fig. 12(b) that the mean and the width of the bands gets higher with the value of V_m. The displacements results become more disperse -and then less predictable- for higher values of V_m, denoted with the warmer and colder colors that can be seen in Fig. 12(b). In Fig. 11(c) three PDFs and different shapes and widths are depicted.

The Figure 13 shows the evolution of the PDF with H_m for the peaks (local maximums), when H is considered stochastic, and for a fixed value of $V_m = 70$ m/s. Fig. 13(b) also contains the (interpolated) confiability bands, although it has a trend to decrease (specially for the lowest and highest values of H_m), the bandwidth remains almost constant. On the other hand, the modes present high variability: in some cases corresponds to the lower values and in other to

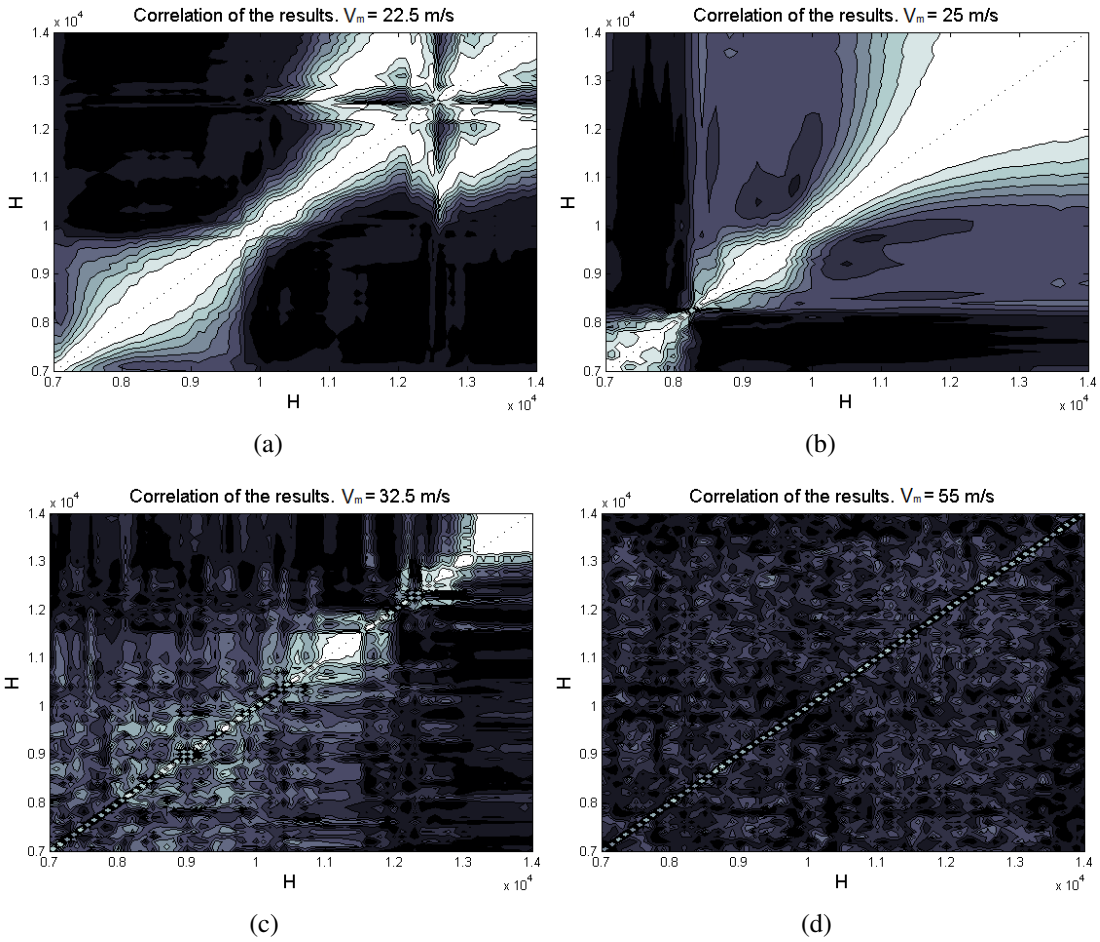

Figure 10: Correlation of the transverse displacement of the beam-column at point $x_b = 0m$ (tip of the mast) found with the deterministic reduced order model for all the combinations of H and four cases of V_m.

the highest, without a clear trend. Other interesting aspect is that the support of the PDFs also present a high variability.

Figure 14 illustrates the evolution of the PDF with V_m for the peaks (local maximums), when H is considered stochastic, and for a fixed value of $H = 7500$ N. The plots in Fig. 14 are quite similar to the one observed in Fig. 12 although the confiability bands are narrow, as well as the support of the PDFs. In this case, there are not multimodalities present.

The plots here presented are representative of a wide spectrum of results. Other plots, with deeper details are not showed here for sake of brevity.

5 FINAL REMARKS

In this work, a nonlinear formulation of a cable-stayed mast structure is presented. First, a deterministic model is stated and the governing system solved via a finite elements discretization. A 2-DOF reduced order model (ROM) of the system is then constructed using eigendata from the previous model. Once calibrated, the ROM was used to perform an uncertainty propagation study using the initial pretension of the cable as a stochastic parameter and a stochastic load to simulate the wind actuating on the mast. The loads take into account spatial and temporal correlations. The study covers a wide range of values of guy pretension and wind mean velocity suggested by the standard codes.The PDFs of the statistic parameters were found by means of the Principle of Maximum Entropy and a Gamma PDF was obtained. Monte Carlo

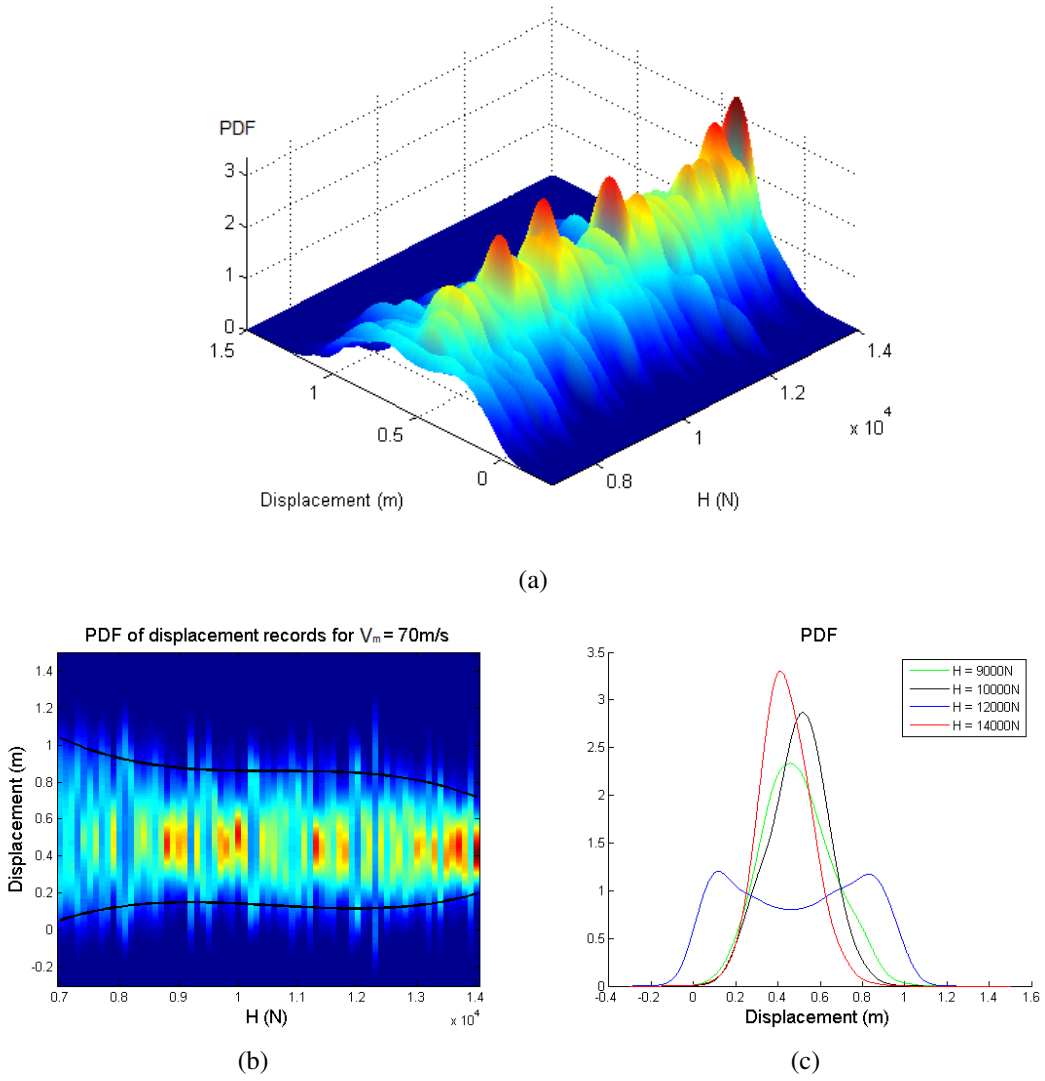

Figure 11: Evolution of the PDF with H of the transverse displacement of the beam-column at point $x_b = 0m$ (tip of the mast) for $V_m = 70$ m/s. (a) 3D plot of displacemnts vs H vs PDF, (b)top view of (a), (c) some cuts of (a)

.

simulations were employed to find the realizations.

First a study on the deterministic response (displacements at the tip of the beam-column) of the deterministic structure with stochastic turbulent load is presented. The overall shape of the time history is discussed and is found that the motion is not periodic, but a deeper analysis would be necessary in order to conclude that is chaotic. The frequency content of the signal is also analyzed and a plot illustrating the variation of the peak frequency with the studied parameters is presented. The most important frequency content for all cases studied is inside the range of $0.5-0.85$ Hz. Phase planes and Poincaré maps were also studied in order to seek for periodic attractors, without remarkable results. The absolute maximum and mean values of each displacement curve are plotted versus H and V_m to determine their influence: is observed that V_m presents a larger heft than H on these measures and with H the variation is less predictable. As an engineering measure, the percentage of time that the displacements surpass a limit value is plotted and it is concluded that for mean wind velocities greater than 55 m/s around the 20%

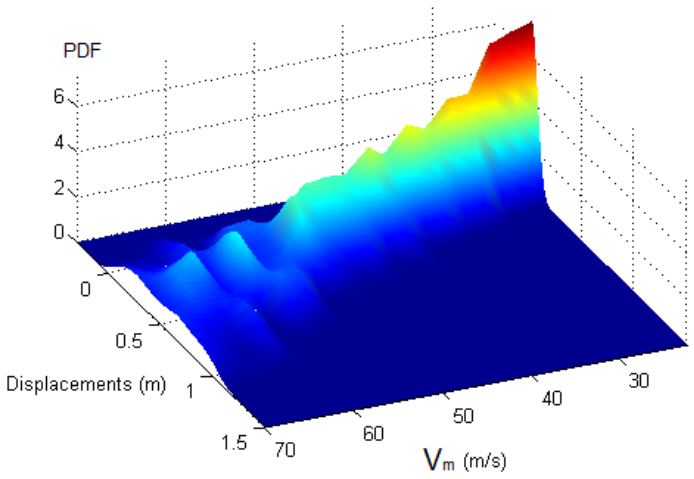

(a)

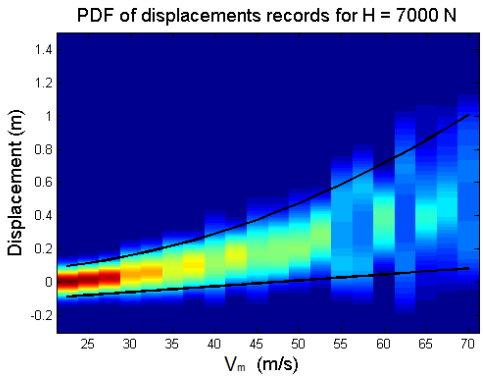

(b)

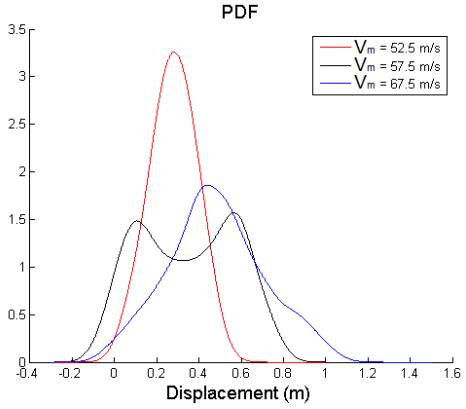

(c)

Figure 12: Evolution of the PDF with V_m of the transverse displacement of the beam-column at point $x_b = 0m$ (tip of the mast) for $H = 7000$ N. (a) 3D plot of displacements vs V_m vs PDF, (b)top view of (a), (c) some cuts of (a)

of the duration of the analysis, the limit value is overpassed, approximately, depending on the value of H.

The results were also studied statistically. The correlation between the time history of displacements is depicted and it is concluded that it is not possible to determine any linear relationship among cases, even with small changes in the parameters. Then, each displacement record is treated as a stochastic process and the evolution of the PDFs, when varying the parameters, is analyzed. When V_m is fixed and the value of H is varied, the mean value of all records remain approximately constant and multimodalities are observed. When H is fixed and the evolution of results with V_m is studied, the dispersion of the results increase rapidly and also multimodalities are present. Then, the local maximums (peaks) are studied, first for a fixed value of V_m and considering H stochastic (and the variation of the results are observed for a wide range of values of H_m): is observed that the width of the bands of confiability is not modified with the value of H_m, also the modes varies from the zone of higher to lower displacements without following any trend. When the value of H_m is fixed (treating H as a stochastic variable) and the results are plotted for all the values of V_m, the absent of multimodalities, previously found for

the studied displacements records is observerd.

6 ACKNOWLEDGEMENTS

The authors acknowledge the financial support from CONICET, MINCyT and UNS (Argentina); CAPES, CNPq, and FAPERJ (Brazil).

REFERENCES

Gattulli V. and Lepidi M. Localization and veering in the dynamics of cable-stayed bridges . *Computers & Structuresl*, 85:1661–1678, 2007.

Lenci S. and Ruzziconi L. Nonlinear phenomena in the single mode dynamics of a cable-supported beam . *International Journal of Bifurcation and Chaos*, 19:923–945, 2009.

Preidikman S., Massa J., and Roccia B. Análisis dinámico de mástiles arriostrados. *Rev. Int. de Desastres Naturales, Accidentes e Infraestructura Civil*, 6(1):85–102, 2006.

Shannon C. A matemathical theory of communication. *The Bell Technical Journal*, 27:379–423, 1948.

Shinozuka M. and Jan C.. Digital simulation of random processes and its applications. *Journal of Sound and Vibration*, 25(1):111–128, 1972.

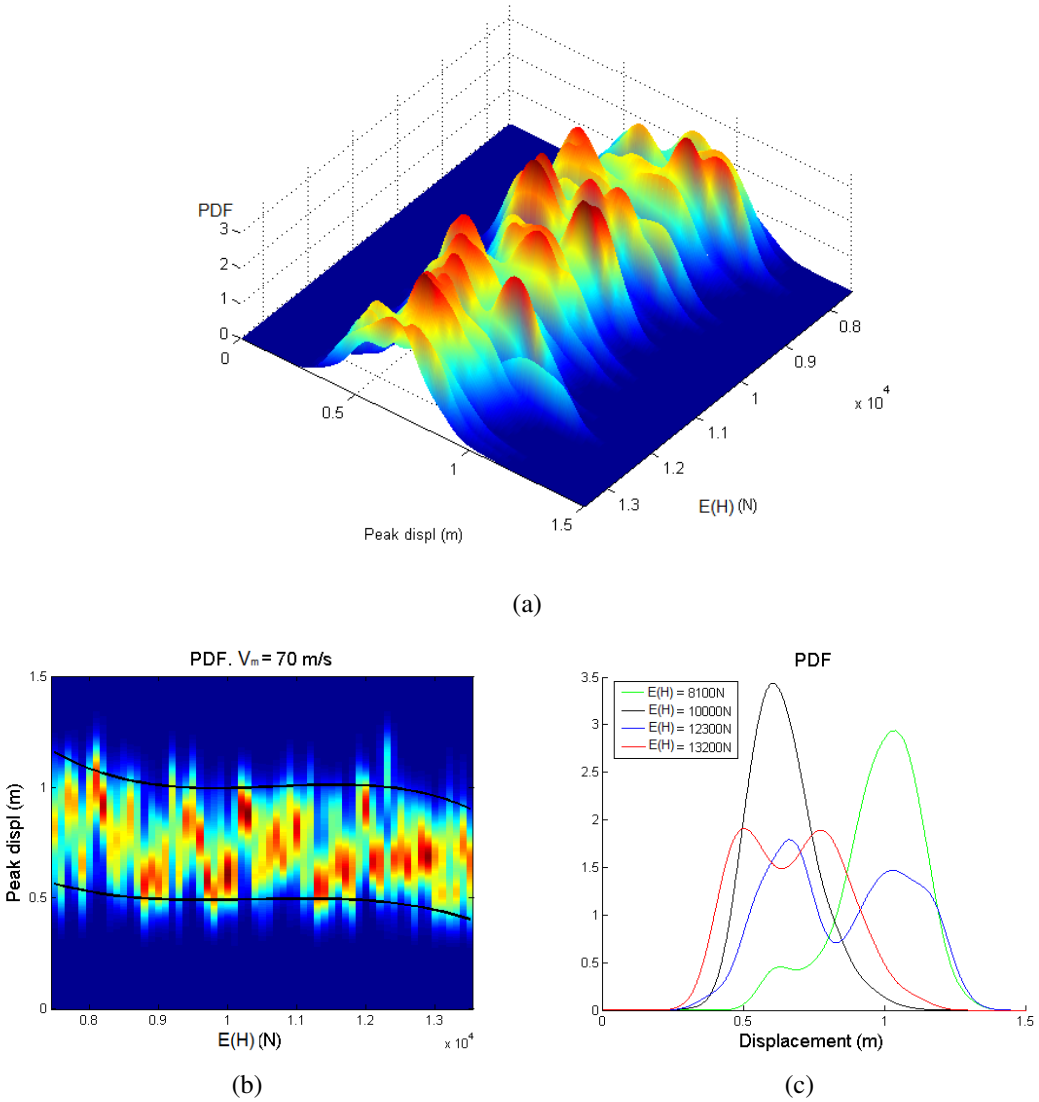

Figure 13: Evolution of the PDF with $E(H)$ (H is considered stochastic, with a Gamma PDF) of the peak values (local maximums)of the transverse displacement of the beam-column at point $x_b = 0m$ (tip of the mast) for $V_m = 70$ m/s. (a) 3D plot of displacemnts vs H vs PDF, (b)top view of (a), (c) some cuts of (a)

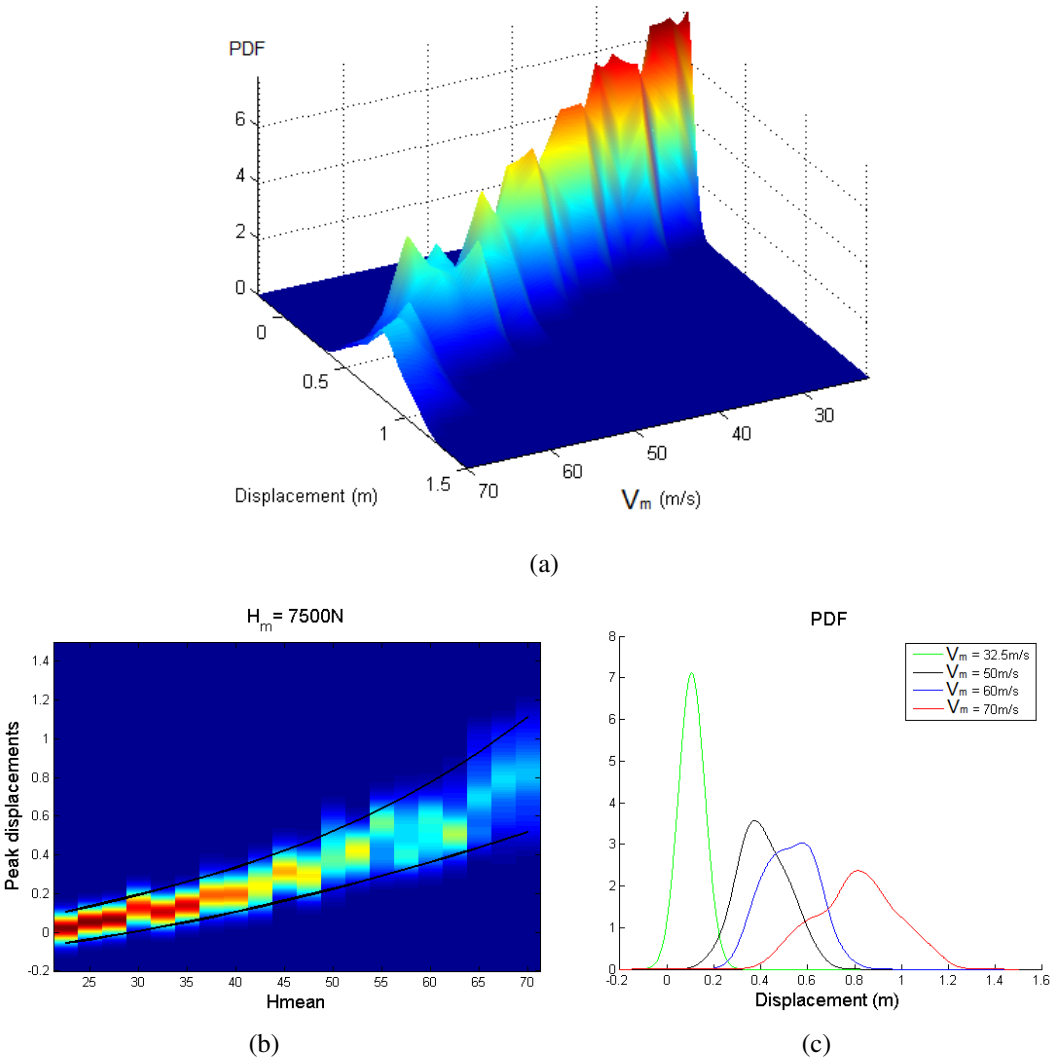

Figure 14: Evolution of the PDF with V_m (H is considered stochastic, with a Gamma PDF and $E(H) = 7500$ N) of the peak values (local maximums)of the transverse displacement of the beam-column at point $x_b = 0m$ (tip of the mast). (a) 3D plot of displacements vs H vs PDF, (b)top view of (a), (c) some cuts of (a)